Ultrasound-Image-Based Cardiovascular Tissue Motion Estimation

Spyretta Golemati, *Member, IEEE*, Aimilia Gastounioti, *Member, IEEE*, and Konstantina S. Nikita, *Senior Member, IEEE*

(Methodological Review)

***Abstract*—The estimation of cardiovascular tissue motion from ultrasound images is a task of considerable importance but has remained difficult in clinical practice, mainly due to the limitations of ultrasound imaging and the complexity of tissue motion. This paper presents a survey of methodologies, along with physiologically relevant findings, regarding the estimation of motion of the myocardium and of central and peripheral arteries. Speckle tracking and modeling, and registration are the dominant methods used to calculate tissue displacements from sequences of images. Kinematic and mechanical indices are extracted from these displacements, which can provide valuable functional information about the cardiovascular system in normal and diseased conditions. An important application of motion-based strain indices involves the estimation of elastograms of the cardiovascular tissue. Motion analysis methods can be used to estimate a number of regional mechanical phenomena representing functional tissue properties, which are more sensitive to early changes due to ageing or disease. The importance of these methods lies in their potential to quantify *in vivo* tissue properties and to identify novel noninvasive personalized disease markers, toward early detection and optimal management of disease, along with increased patient safety. Their clinical usefulness remains to be demonstrated in larg trials.**

***Index Terms*—Cardiology, motion estimation, ultrasonography.**

I. Introduction

CARDIOVASCULAR disease (CVD), caused by disorders of the heart and blood vessels, is the number one cause of death globally and is projected to remain the leading cause of death [1]. If appropriate action is not taken, by 2030 more than 23 million people will die from CVD every year, mainly from heart attacks and strokes. People with CVD, or, at high CVD risk due to the presence of one or more risk factors, need early detection and management.

Manuscript received November 1, 2015; revised February 5, 2016; accepted March 23, 2016. Date of publication April 25, 2016; date of current version September 16, 2016.

S. Golemati is with the Medical School, National Kapodistrian University of Athens, Athens 10675, Greece (e-mail: sgolemati@med.uoa.gr).

A. Gastounioti is with the School of Electrical and Computer Engineering, National Technical University of Athens, Athens 15780, Greece, and also with the Department of Radiology, University of Pennsylvania, Philadelphia, PA 19104 USA (e-mail: gaimilia@biosim.ntua.gr).

K. S. Nikita is with the School of Electrical and Computer Engineering, National Technical University of Athens, Athens 15780, Greece (e-mail: knikita@ece.ntua.gr).

Digital Object Identifier 10.1109/RBME.2016.2558147

Clinical diagnosis, treatment, and follow up of CVD are greatly aided by a number of imaging techniques that provide qualitative and quantitative information about morphology and function of the heart and the blood vessels. Furthermore, advanced image processing methods can be used to extract features from images and facilitate image interpretation and subsequent decisions on disease management [2]. Among such features, the estimation of motion of the myocardial and arterial walls is important for the quantification of tissue elasticity and contractility and has gained attention as a determinant of CVD [3]. Myocardial and arterial wall elasticity is altered with age as well as in the presence of pathology (e.g., atherosclerosis, diabetes, and renal disease) mainly due to changes in wall composition.

Ultrasound imaging is widely used in the diagnosis of CVD because it allows noninvasive assessment of disease severity and tissue morphology. Modern ultrasound systems allow real-time imaging of moving structures as well as storage of temporal image sequences, or cine loops, for further processing. Tissue motion can be quantitatively estimated from these sequences provided they are acquired at sufficiently high frame rates. Radio frequency (RF) and brightness (B) mode are the appropriate modalities for studying tissue motion in two or in three dimensions. Compared to RF signals, B-mode signals have reduced information content and, as a result, require reduced storage capabilities.

The estimation of cardiovascular tissue motion from ultrasound images is a task of considerable importance but has remained difficult in clinical practice. Objective evidence that contractility is normal in patients examined at screening may be as important as the reliable quantification of ventricular and arterial function and the detection of wall-motion abnormalities at rest or during stress in those with suspected CVD. However, ultrasound imaging is not an easy modality for interpretation. Tissue motion is complex, encompassing thickening, translation, rotation, and shear. In addition to this, unlike other imaging modalities, ultrasound images suffer from speckle noise, which tends to reduce the image contrast and image details, and from an inherent tradeoff between spatial resolution and penetration depth, which both degrade the quality of images. Furthermore, anatomical borders lack continuity, which, together with the above limitations, significantly limits the applicability of standard image analysis approaches.

In this paper, a survey was attempted of the methodologies used in previous studies, along with the reported physiologically relevant findings, regarding the estimation of cardiovascular

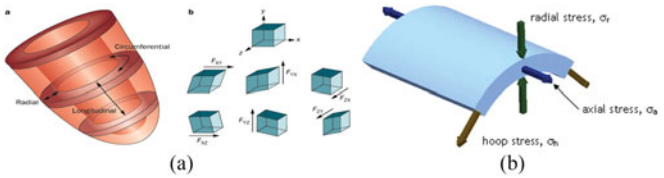

Fig. 1. Illustration of (a) myocardial deformation in three dimensions and (b) different arterial stresses (The image in (a) was taken from [13] and the one in (b) from [76].).

tissue motion from sequences of ultrasound images. In the context of this survey, important aspects of the investigated area are highlighted, including the mechanical phenomena underlying tissue motion estimation, and technical aspects important for the reliable acquisition of data and interpretation of results. Such a systematic collection and organization of previous works are expected to serve not only as a purely informative report but also as a useful guideline for future studies in this continuously growing field.

II. Motion of the Cardiovascular Tissue

Myocardial and arterial tissue deformations are both due to the periodic movement of the heart. A normal heart initiates an electrical potential that causes the muscle to contract. In the resting state, the heart muscle is an inhomogeneous, anisotropic, incompressible, and viscoelastic material [4]. The myocardial deformation is mainly guided by an internal contractile force and the tissue elasticity which translates in the fiber/matrix structure and the presence or absence of fibrosis and depositions. However, any part of the myocardium is always imbedded in a ventricle; therefore, the intracavity pressure and the interaction with neighboring contracting segments are additional important influencing factors for the myocardial deformation [see Fig. 1(a)].

Arteries *in vivo* are in constant movement because they are subjected to constantly changing stresses due to pressure oscillations associated with each cardiac cycle. Arterial movement consists of rapid distension during ventricular ejection, whereby 50% or more of the stroke volume is transiently accommodated, and of retraction during diastole. When arteries are pressurized, they are subjected to distension in all directions, i.e., circumferential (or hoop stress), longitudinal (or axial), and radial directions [see Fig. 1(b)]. Strains and stresses in the circumferential and longitudinal directions are tensile because the vessel tends to distend in these directions with pressurization. Strains and stresses in the radial direction are compressive as the wall tends to be narrowed with pressurisation.

The largest strains have been reported in the circumferential direction, corresponding to vessel diameter changes, and the lowest in the radial direction, corresponding to wall thickness changes. Specifically, most conduit arteries undergo 8%–10% oscillation in external diameter or about 15% oscillation in internal diameter. Of particular interest seem to be strains in the longitudinal direction. These have gained but little interest because they were assumed to be negligible compared to circumferential strains (CS) [5]. However, recently, with modern ultrasound scanners and reliable motion estimation algorithms, it was shown that longitudinal movement of the common carotid artery was comparable to the diameter change [6], [7]. It is pointed out that longitudinal strains (LS) result from the effect of perivascular connective tissue and from the effect of constraint provided by arterial side branches. This constraint has been termed "tether."

In large arteries, the stability, resilience, and compliance of the vascular wall, i.e., its mechanical properties, are dependent on the relative contributions of its two main structural proteins: collagen and elastin. The former provides the tensile strength of the wall, and, thus, its structural integrity, whereas the latter provides elasticity; both are potently regulated by catabolic matrix metalloproteinases. Ageing, as well as the presence of a number of diseases, including atherosclerosis, diabetes, and chronic renal disease favor the development of arterial stiffness [8]. Increased stiffness reduces the reservoir function of the conduit arteries near the heart and increases pulse wave velocity, thus increasing systolic and pulse pressures. Given that these two pressures determine the peak loads on the cardiovascular system, their increase has an unfavorable effect on the system strength [8].

III. Measurement of Tissue Motion

A wide variety of methods have been proposed to estimate tissue motion and strain, shedding light on the understanding of cardiovascular physiology and mechanics. These methods can be broadly classified as: 1) speckle tracking and 2) image registration. Speckle tracking was the descendant of tissue Doppler imaging (TDI), which, by allowing angle independent tissue velocities in the entire ultrasound image, it successfully addressed a major limitation that only the velocity component in the direction of the ultrasound beam could be determined. Image registration is a more recent methodology, which is also receiving growing attention.

Ultrasound images are generated by the reflection of coherent ultrasound waves, which are transmitted from a transducer into the body. Speckle is the result of the interaction between those waves and different types of tissues, and is produced by interfering echoes of a transmitted waveform that emanate from tissue heterogeneities [9]. Specifically, speckle is caused by waves scattering off small particles in the tissue being scanned and alternately reinforcing and then cancelling each other. Speckle tracking methods analyze motion by tracking the intensity or the interference patterns produced by speckle over time. Therefore, to estimate tissue motion and strain using speckle tracking, one needs: 1) a sequence of ultrasound images appropriately recorded and 2) a reliable speckle tracking method.

The main technical considerations to be incorporated in cardiovascular tissue motion analysis protocols correspond to constraints imposed by: 1) arterial wall physiology, which affects subject and probe setup; and 2) physical principles of ultrasound imaging, which affect selection of scanner setting values. These should be taken into account for reliable recording of tissue motion using ultrasound imaging. Then, the quantitative analysis of tissue displacement is performed with the application of the speckle tracking algorithm to the recorded image sequence.

A number of speckle tracking methods, including block matching (BM) and differential methods, have been used for cardiovascular tissue displacement estimation. This particular class of algorithms is very popular in this research field with several applications for different cardiovascular pathologies and therapies. However, their performance is usually limited by tissue deformation, and the resulting decorrelation, and, in two-dimensional (2-D) image recordings, out-of-plane motions [10]. Both these factors may substantially modify image patterns over time, and, therefore, limit the ability of speckle tracking methods to correlate consecutive frames.

Image registration overcomes the aforementioned limitation of speckle tracking. Image registration methods estimate motion by frame-to-frame or groupwise registering successive ultrasound frames with a deformable shape tracking approach. The deformation field is parameterized using smooth basis functions, often B-splines in image processing. Adding extra cost terms to the energy function to be optimized then typically regularizes the motion.

Speckle tracking and image registration methodologies generate vectors, which can be processed so as to extract quantitative indices. Motion vectors corresponding to displacements of individual image areas over the total duration of the recording can be quantified in terms of amplitude, frequency, or in the case of pairs of areas, the synchronization. Standard indices include radial (RS), LS, CS, and shear (SS) strain indices, as well as distensibility or compliance indices, when pressure measurements are available.

As opposed to the previously presented intensity-based methods, phase-based approaches consist in processing the information carried by the phase of the images, namely in the frequency domain. Another alternative to the previous approaches is the formulation of optical flow, one of the differential speckle tracking methods, in polar coordinates. This formulation highlights additional motion information, and maybe preferable in specific geometry cases, such as cylindrical shapes.

A major application of motion analysis is elastography, a quantitative method for imaging the elasticity in biological tissues, introduced in the early nineties by Ophir *et al.* [11]. The method consists of calculating 2-D local tissue strain through cross correlation of RF segments for the estimation of the time shift resulting from inherent deformations. Strain represents the displacements of tissue particles with respect to a reference position, and is the parameter that is mapped with conventional elastography. The more recently suggested shear-wave elastography maps elastic moduli, i.e., the ratio of stress and strain, where stress is induced by the shear wave of the device.

IV. Clinical Applications

Clinical applications of cardiovascular tissue motion estimation include: 1) the heart, namely the myocardium, 2) the central vessels, namely the aorta and the coronary arteries, and 3) peripheral arteries, namely the carotid, the brachial, femoral, and popliteal arteries. With the exception of coronary arteries, transcutaneous ultrasound is used to image all other cardiovascular structures; intravascular ultrasound (IVUS) is used to image the coronaries [12]. Transoesophageal ultrasound is sometimes used to image the central vessels, and produces clearer images than transcutaneous ultrasound. Table I summarizes the studies that suggested methods for estimation of cardiovascular tissue motion.

A. Myocardium

Accurate characterization of myocardial motion patterns is essential for understanding changes in cardiac mechanics under the effect of disease and therapy [13], [14]. The quantification of myocardial deformation, especially when combined with the response to a dobutamine challenge, has been associated with a valuable role in the detection of regional abnormalities and in the diagnosis of different cardiac pathologies, such as mitral regurgitation [15], ischaemia [16], [17] and dyssynchrony [18] (see Fig. 2). In particular, the strain and the strain rate (i.e., speed at which deformation occurs) have been commonly used to assess the regional and global (calculated by averaging values in multisegment models) myocardial function [19].

Saltijeral *et al.* associated motion indices with obesity cardiomyopathy [20]. Using a dataset of 30 obese children and 42 healthy volunteer children, it was shown that 3-D speckle tracking provides kinematic parameters (strain, twist, and torsion) which are able to assess the presence of early myocardial deformation abnormalities due to obesity. This conclusion suggested that obesity cardiomyopathy, which is a major risk factor for cardiovascular morbidity and mortality, is associated not only with structural cardiac changes, but also with myocardial deformation changes, and that this association occurs as early as in the childhood and it is independent from any other cardiovascular risk factor.

Speckle tracking was also used to measure regional and global (calculated by averaging strain values in a 16-segment model) LS in 20 patients with acute ST elevation myocardial infarction and relatively preserved left-ventricular function [21]. The reported findings indicated that both regional and global LS might provide an accurate assessment of global myocardial function and of the presence of segments with transmural extent of necrosis.

Furthermore, speckle tracking holds a valuable role in revealing motion and deformation changes induced by pure left-bundle-branch block (LBBB) and their evolution with cardiac resynchronization therapy (CRT) [22]. In this study, myocardial displacement, velocity, and strain were estimated for 22 swine models of acute LBBB and CRT with ($N = 11$) or without ($N = 11$) chronic infarct, and were used as input toward estimating indices of mechanical dyssynchrony. Most animals without infarct showed uniform intraventricular dyssynchrony patterns and recovery toward a normal pattern with CRT. Variability in LBBB-related mechanical dyssynchrony patterns was high in infarct presence, which also affected the CRT efficiency (improvements in 6/11 animals).

The value of speckle tracking was also demonstrated in combination with low dose dobutamine stress echocardiography for the evaluation of viable myocardium in patients with acute myocardial infarction [23]. Speckle tracking was used to

TABLE I
SUMMARY OF METHODS FOR ESTIMATION OF CARDIOVASCULAR TISSUE MOTION

Study	Method	Validation/Evaluation	Derived measures	Clinical applications
		Myocardium		
Saltijeral *et al.* [20]	speckle tracking	–	strain, twist, torsion	obesity cardiomyopathy is associated with myocardial deformation changes
Cimino *et al.* [21]	speckle tracking	–	global and regional LS	global and regional LS can accurately assess global myocardial function and the presence of segments with transmural extent of necrosis
Duchateau *et al.* [22]	speckle tracking	–	displacement, velocity, strain (and derived indices of dyssynchrony)	variability in LBBB-related mechanical dyssynchrony patterns was high in infarct presence, which also affected the CRT efficiency
Gong *et al.* [23]	speckle tracking	–	LS and LS rate	LS and LS rate were independent predictors of viable myocardium, while combining LS and LS rate with dose dobutamine stress echocardiography further enhanced the predictive ability for myocardial viability
Alessandrini *et al.* [24]	monogenic signal theory	synthetic sequences	displacements, strains	higher accuracy, superior robustness to the noise, and shorter computation time compared to state-of-the-art speckle tracking approaches
Curiale *et al.* [25]	diffeomorphic speckle tracking	synthetic images	strain	valid identification of abnormal segments with reduced cardiac function and timing differences for dyssynchrony cases
Duchateau *et al.* [26]	nonrigid registration	synthetic images	strain	valid quantification of motion abnormalities at every location in time and space
Bosch *et al.* [32]	AAMMs	*in vivo* data	eigenvariations of shape/motion	significant associations with volumetric measures of ventricular dilatation
Lee and Konofagou [33]	cross correlation	*in vivo* data	strain	reliable localization of the early onset of myocardial ischaemia [34] accurate differentiation between different motion schemes, sensitivity to stiffness changes [35]
		Aorta		
Luo and Konofagou [36]	1-D cross correlation	human aorta *in vivo*	displacements	in murine aneurysmal aortas, wall motion was reduced and spatially varied, and more asynchronous with blood flow, compared to normal aortas [37] estimation of strain to derive the stress–strain curve [38]
		Coronary arteries		
de Korte *et al.* [40]	cross correlation	comparison with histology	strain	high strain values (1%–2%) in soft plaques, but low strain values (0%–0.2%) in calcified material [41]
Maurice *et al.* [42]	LSME	simulated RF data	radial strain	low and high strain/shear values, corresponding to hard and soft plaque materials, respectively, were found in different human plaque types [43], reconstruction of atherosclerotic plaque elasticity from radial strain sequences [44]
Liang *et al.* [45]	2-D nonrigid registration PVA phantom	synthetic motion of IVUS images of porcine carotid artery	radial and CS distributions	LAD coronary artery [46] lesion stiffness was consistent with tissue composition from histological cross sections [47]
Liang *et al.* [48]	3-D nonrigid registration	IVUS images of healthy porcine carotid arteries	strain distributions	the algorithm was able to overcome systematic noise and provide consistent results under different resolutions
		Carotid arteries		
Golemati *et al.* [49]	BM	*in vivo* data	radial and longitudinal displacements	arterial wall distensibility in the radial direction was significantly higher than in the longitudinal direction
Cinthio *et al.* [50]	BM	*in vitro* (phantom) data	displacements, strains	bidirectional longitudinal movement of the IM complex during the cardiac cycle [6]
Zahnd *et al.* [52]	BM	*in vivo* data	radial and longitudinal displacements	displacements were significantly lower in elderly diabetic subjects longitudinal motion was impaired in the presence of periodontal disease [53]
Soleimani *et al.* [54]	BM	–	longitudinal stress	strong and graded association between axial stress and severity of carotid stenosis
Gastounioti *et al.* [7]	adaptive BM	in silico and *in vivo* data	displacements, strains	carotid motion and strain can discriminate between symptomatic and asymptomatic patients [56], both the atherosclerotic lesion and the normal wall adjacent to the lesion should be considered
Zahnd *et al.* [57]	BM+KF		longitudinal motion amplitude	longitudinal motion amplitude was significantly reduced at high-risk patients compared with healthy volunteers, longitudinal motion amplitude was progressively attenuated along the length of the artery [58]
Tat *et al.* [59]	multikernel BM + KF	–	displacements, strains	compared with able-bodied subjects, the retrograde intramural SS was significantly smaller in individuals with SCI, smaller peak displacements in both the IM and adventitia
Albinsson *et al.* [60]	BM with additional reference block	in silico phantom and *in vivo* data	Longitudinal movement	improved tracking performance using the suggested approach
Maurice and Bertrand [61]	LSME	simulated RF images	2-D strain tensor	computation of elastograms of carotid artery [62]
Svedlund and Gan [64]	VVI	*in vivo* data	longitudinal displacements	longitudinal displacements in the normal common carotid artery were significantly lower in subjects with CAD compared to healthy young adults, in mice, low longitudinal displacements were associated with greater IMT, greater plaque burden, and higher cholesterol levels [65],

TABLE I
(Continued)

Study	Method	Validation/Evaluation	Derived measures	Clinical applications
				longitudinal displacements predicted short-term event-free survival in medium- to high-risk patients [66]
Golemati *et al.* [67]	BM, OF	in silico and *in vivo* data	radial, LS, and SS	radial strain decreases with age, differences in phase and amplitude between RS, LS, and SS waveforms
Mokhtari-Dizajl *et al.* [68]	OF	–	arterial stiffness indices	differences in arterial stiffness between subjects with severe stenosis compared to subjects with mild or no stenosis
Zahnd *et al.* [71]	phase-based OF	*in vivo* data (comparison with manual trajectories)	longitudinal and radial motion amplitudes	improved tracking performance with the suggested beamforming strategy
		Other peripheral arteries		
Cinthio *et al.* [6]	BM	*in vivo* data	longitudinal displacements	bidirectional longitudinal movement of the IM complex during the cardiac cycle, SS between IM and adventitia

AAMM: active appearance motion model; BM: block matching; CRT: cardiac resynchronisation therapy; IM: intima-media; IMT: IM thickness; IVUS: intravascular ultrasound; KF: Kalman filtering; LBBB: left-bundle-branch block; LS: longitudinal strain; LSME: Lagrangian speckle model estimator; OF: optical flow; PVA: polyvinyl alcohol; RF: radiofrequency; TDI: tissue Doppler imaging; VVI: vector velocity imaging.

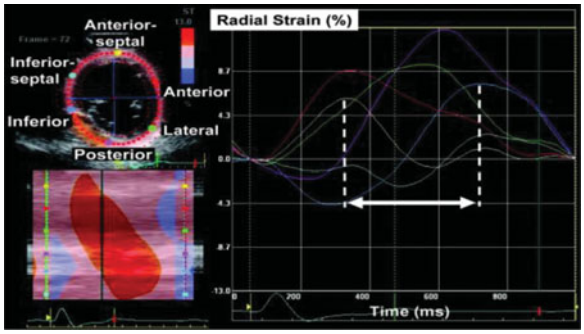

Fig. 2. Example of radial time–strain curves in a heart failure study patient with LBBB. Radial strain was calculated by speckle tracking and averaged to six time–strain plots to represent standard segments. The curves are color coded by the defined myocardial regions as depicted in the figure (yellow = anterior septum; red = anterior segment; green = lateral; purple = posterior; dark blue = inferior; and light blue = septum). An example of dyssynchrony is shown as the difference in timing of peak strain from earliest to latest segment (white arrow). Dyssynchrony for this study was defined as a time difference ≥130 ms between the anterior septal and posterior wall peak strain (from [18]).

measure end-systolic strain and peak-systolic strain rate of regional wall motion abnormality segments in 42 patients one, three, and six months after percutaneous coronary intervention. Among the speckle tracking measurements, LS and LS rate (LSr) emerged as independent predictors of viable myocardium, while combining LS and LSr with dose dobutamine stress echocardiography further enhanced the predictive ability for myocardial viability.

In an attempt to further upgrade the role of the popular speckle tracking approaches, Alessandrini *et al.* attempted to overcome limitations by the variation of image intensities over time due to myocardial motion and out-of-plane motions. To this end, they proposed a motion estimator, which is based on monogenic signal theory and decouples the local energy from the image structure, accounted for by phase and orientation [24]. The validation of the proposed algorithm against state-of-the-art speckle tracking approaches in realistic synthetic sequences of cardiac ultrasound images showed higher accuracy, superior robustness to noise, and a considerably shorter computation time.

Another attempt to enhance the performance of speckle tracking was recently published by Curiale *et al.* [25]. The authors proposed a maximum-likelihood approach, which generalizes conventional speckle models to a more versatile model for real data, increases the efficiency of frame-to-frame speckle tracking, and identifies more reliable myocardial motions. In the framework of a comparative evaluation on 16 synthetic image sequences for three different scenarios (normal, acute ischaemia, and acute dyssynchrony), the proposed methodology outperformed previously presented speckle tracking methods by minimizing the median motion and strain error in the circumferential, longitudinal, and radial direction of motion. It also showed great potential in identifying abnormal segments with reduced cardiac function and timing differences for the dyssynchrony cases.

Elastic (nonrigid) registration solutions for assessing myocardial strain in ultrasound have also received increasing attention. Duchateau *et al.* used elastic registration to generate velocity fields, which were then used to build a subject-specific statistical atlas of motion, allowing the comparison of patients against the atlas using quantitative indices of abnormality [26]. This methodology was applied to 21 healthy subjects and 14 CRT candidates with left ventricular dyssynchrony and demonstrated great potential in quantifying motion abnormalities at every location in time and space.

Moreover, in a recently published *in vivo* setting [27], registration based methodologies were evaluated against speckle tracking by comparing both to a gold standard reference measurement (sonomicrometry). RS, LS, and CS were estimated in four sheep during four stages (i.e., at rest, during esmolol and dobutamine infusion, and during acute ischaemia) by applying two well-validated speckle tracking [28] and elastic registration [29] approaches. The correlations of RS and CS with sonomicrometry were comparable for the two methodologies. However, the elastic registration method, the core of which was the enforcement of time consistency using spatiotemporal B-

spline kernels [29], considerably outperformed speckle tracking for LS.

Furthermore, wall motion abnormalities in cardiac ultrasound have been examined using active shape models (ASMs) [30], which are statistical shape models that iteratively deform to fit to a new image, and active appearance motion models (AAMMs) [31], [32], which are an extension of ASMs describing both the appearance and the shape of the myocardium. As an example, an automated AAMM-based approach for left ventricular endocardial border detection [31] was applied to a set of stress echocardiograms of 129 infarct patients and the eigenvariations of shape/motion were found to be associated with volumetric measures of ventricular dilatation [32].

Last, myocardial elastography has demonstrated great potential in noninvasively assessing regional myocardial function, with the advantages of high spatial and temporal resolution and high signal-to-noise ratio. Myocardial elastography is an RF-based technique [12], [33]–[35], which has been developed to map the 2-D transmural deformation field and detect abnormal cardiac function. Cross correlation is used to calculate tissue displacements and derive strains. *In vivo* studies using myocardial elastography showed that it allows reliable characterization and differentiation of abnormal from normal myocardia [33] and localization of the early onset of myocardial ischaemia [34], without any angular dependence. Moreover, in a recent study applying myocardial elastography to phantoms subjected to four motion schemes (rotation, torsion, deformation, and a combination of torsion and deformation) [35], the methodology was found to be capable of accurately distinguishing between different motion schemes, and to be sensitive to stiffness changes in localized phantom regions under physiologic cardiac motion configurations.

B. Aorta

Visualization of aortic wall pulsation with ultrasound has allowed the description of aortic wall motion as a change in diameter (or cross-sectional area) during pulsation. Development of image analysis methods, such as cross correlation, has enabled more detailed study of arterial wall motion. With these techniques, not only diameter change but also strain parameters along an arterial segment can be evaluated, offering the prospect of individual noninvasive rupture risk analysis of abdominal aortic aneurysms.

Luo and Konofagou proposed a method based on sum tables for fast calculation of the normalized correlation coefficient (NCC) in ultrasound-based motion estimation [36]. Both the numerator and denominator in the NCC definition were obtained through precalculated sum tables to eliminate redundancy of repeated NCC calculations. The method was evaluated using RF signals from a human abdominal aorta *in vivo*. The method was subsequently used to investigate the synchrony between wall motion and blood flow in murine normal and aneurysmal aortas [37]. These two parameters were uniform and synchronous in normal aortas, but reduced, spatially varied and less synchronous in aneurymal aortas. Furthermore, it was used to estimate tissue strains from RF images of murine arteries and assess stress–strain curves, in combination with stress estimates obtained from applanation tonometry [38]. The methodology was later used in the carotid arteries of young norma adults [39].

C. Coronary Arteries

In coronary arteries, motion estimation methodologies have been applied to calculate strains and elastograms from IVUS images. These methodologies include cross correlation, the Langrangian speckle motion estimator (LSME), as well as 2-D and 3-D nonrigid registration.

de Korte *et al.* suggested the application of cross correlation in echogram pairs acquired at two different intravascular pressures [40]. The resulting tissue displacements were converted to strain. The method was validated by matching strain to histology; fibrous tissue was hardest, whereas fatty components were softest. It is important to point out that these plaque types did not reveal echodensity differences on the corresponding echograms. Additionally, investigation of the predictive value of the method for identifying the vulnerable plaque showed that a high strain region at the lumen vessel wall boundary had 88% sensitivity and 89% specificity for identifying such plaques [41]. The presence of a high strain region at the lumen-plaque interface has a high predictive value for identifying macrophages. Patient studies revealed high strain values (1%–2%) in soft plaques, whereas calcified material showed low strain values (0%–0.2%).

Maurice *et al.* suggested using LSME for computation of strains from endovascular ultrasound elastography [42]. The method was implemented through an adapted version of the Levenberg–Marquardt minimization algorithm, using the optical flow equations formulated in a polar coordinate system. It was also validated with simulated ultrasound RF data of mechanically complex vessel wall pathologies. The same approach was subsequently used to estimate elastograms of RS and RS distributions within the vessel wall [43]. Low and high strain/shear values, corresponding to hard and soft plaque materials, respectively, were found in different human plaque types. The LSME methodology was subsequently applied to reconstruct atherosclerotic plaque elasticity from coronary IVUS radial strain sequences in 12 patients referred for coronary atherectomy [44].

In an attempt to enhance elastography procedures and estimate the strain tensor of the arterial wall from IVUS images, Liang *et al.* suggested a nonrigid-registration-based approach [45]. The method registers a pair of images acquired at a vessel site under different levels of luminal pressure and estimates the 2-D displacement field in the vessel cross section. The displacement field is then used to calculate the 2-D local strain tensor. By means of experiments using synthetic motion of IVUS images of porcine carotid artery and PVA phantom, they demonstrated that the suggested method can efficiently estimate RS and CS of the arterial wall. Fig. 3 shows examples of displacements in synthetic data. They subsequently applied the method to real IVUS images of a LAD coronary artery acquired clinically in continuous pullback mode [46]. Furthermore, they investigated the correspondence between coronary arterial strain, including RS, CS, and SS, and histology in a porcine model of atherosclerosis [47]. They found that lesion

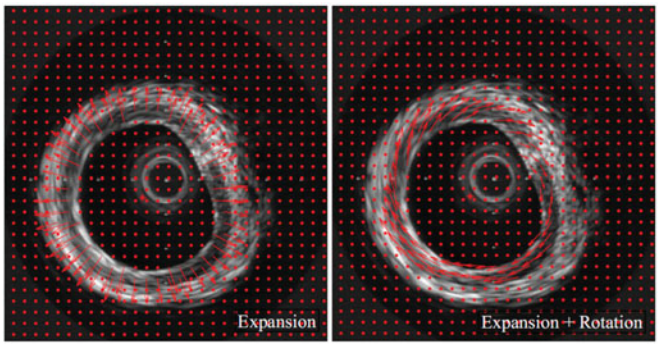

Fig. 3. Examples of calculated displacement field after image registration in synthetic motion experiments: in the case of (left) expansion only and (right) expansion and rotation (from [45]).

stiffness was consistent with the tissue composition seen in the histological cross sections. The method was extended to 3-D, by registering image volumes, and calculated radial, circumferential, and longitudinal displacements [48]. It was validated and evaluated using IVUS images of healthy porcine carotid arteries subjected to a luminal pressure increase and longitudinal stretch.

D. Carotid Arteries

Motion of the normal and diseased carotid artery wall is important in the diagnosis of carotid atherosclerosis. Radial as well as longitudinal motion of the normal, i.e., nonatherosclerotic common carotid artery has been estimated from longitudinal sections not only in normal arteries but also proximal to plaque. Motion patterns of the plaque itself have also been described and associated with the risk for cerebrovascular complications, such as strokes or transient ischaemic attacks.

BM has been used by a number of groups to estimate motion of the carotid artery and associate it to the presence of disease. Golemati *et al.* showed that arterial wall distensibility in the radial direction was significantly higher than distensibility in the longitudinal direction ($10.2 \pm 4.5\%$ versus $2.5 \pm 0.89\%$) [49], which is indicative of tissue anisotropy. Cinthio *et al.* demonstrated that the reproducibility of their BM-based method was 0–8 μm for the radial and 0–12 μm for the longitudinal direction [50]. The intraobserver variability was also estimated *in vivo*, in terms of a coefficient of variation, which was less than 16% for displacements and somewhat higher (24%) for intramural SS measurements [51]. Experiments in healthy humans showed a distinct bidirectional longitudinal movement of the intima-media complex during the cardiac cycle [6]. Zahnd *et al.* found that amplitudes of radial and longitudinal displacements of the near and far arterial walls were significantly lower in elderly diabetic subjects compared to healthy volunteers [52]. The same group also showed that carotid longitudinal motion was impaired in the presence of periodontal disease [53]. Last, Soleimani *et al.* generated BM-based longitudinal motion waveforms of healthy subjects and of patients with less and more than 50% carotid artery stenosis and they reported a strong and graded association between axial stress and severity of carotid stenosis [54].

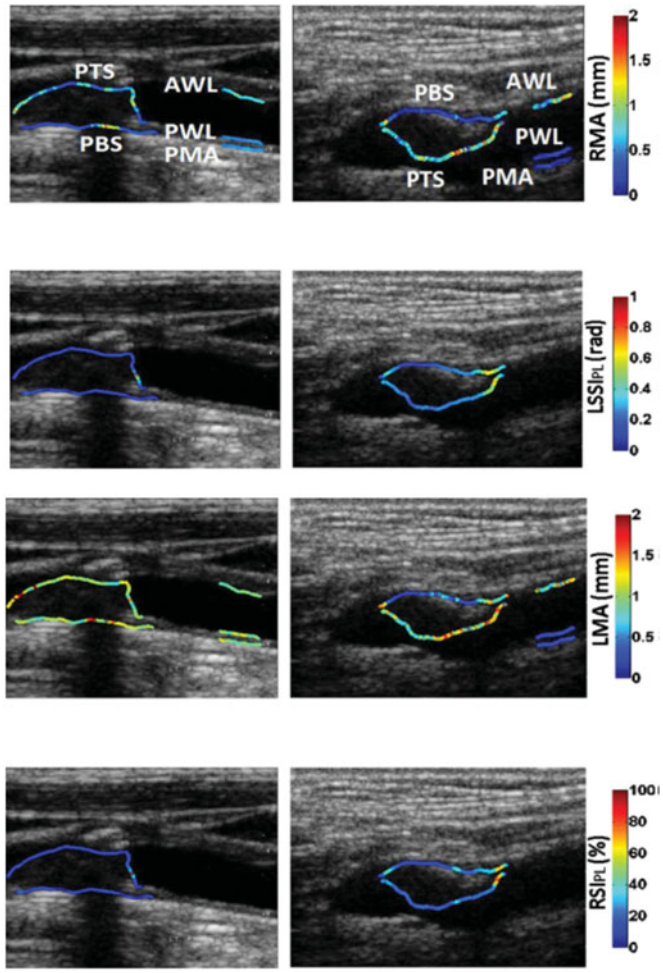

Fig. 4. Examples of color-coded distributions of various motion-derived indices for an asymptomatic (left column) and a symptomatic (right column) patient with an atherosclerotic plaque on the posterior and the anterior wall, respectively. White labels indicate the selected ROIs for each case. RMA/LMA: radial/longitudinal motion amplitude; $\mathrm{LSSI_{PL}}$: longitudinal strain index at plaque; $\mathrm{RSI_{PL}}$: radial strain index at plaque (from [7]).

To improve the performance of BM, a number of advanced alternatives have been suggested. Our group has designed a number of speckle tracking motion estimators, which incorporate adaptive strategies able to handle the major limitation of speckle tracking, i.e., the varying image intensities over time [7]. The motion estimators were evaluated using an *in silico* framework, consisting of 13 computer-generated image sequences that simulate realistic scenarios of ultrasound image recordings. Among the examined adaptive strategies, highest performance, in terms of both accuracy in motion tracking and computational efficiency, was observed for adaptive strategies, which are based on finite impulse response filtering or Kalman filtering [7], [55]. Fig. 4 shows examples of color-coded distributions of motion-derived indices. The *in vivo* application of those algorithms to patients with symptomatic and asymptomatic carotid atherosclerosis was among the first studies that revealed the discriminatory capacity of carotid motion and strain, showing also that the deformation of both the atherosclerotic lesion and the normal wall adjacent to the lesion should be considered [56].

Kalman filtering was also incorporated in speckle tracking by a later study of Zahnd *et al.* [57]. The proposed algorithm was validated using manually traced reference trajectories as groundtruth, and its accuracy was of the same order of magnitude as the inter- and intraobserver variability, and smaller than for six previously proposed speckle tracking methods. The estimated longitudinal motion amplitude was significantly reduced at high-risk patients compared with healthy volunteers, suggesting that this measure may assist early-stage atherosclerosis detection. Another interesting finding was derived by the recent application of the same algorithm to healthy common carotid arteries, where the longitudinal motion amplitude was found to be progressively attenuated along the length of the artery, as it was larger in regions located closer to the heart and smaller in regions located toward the head [58].

The combination of BM with Kalman filtering was also recently followed by Tat *et al.* [59]. The authors applied a multikernel adaptive BM algorithm to assess the longitudinal motion of the common carotid artery in seven individuals with spinal cord injury (SCI), considered at high risk of CVD, and in seven able-bodied participants. Bidirectional movement patterns containing motion retrograde to blood flow during systole, followed by antegrade motion during diastole, characterized longitudinal motion. The retrograde intramural SS was significantly smaller in individuals with SCI by 60.2%, showing smaller peak displacements in both the intima—media and adventitia, while in the antegrade direction, there were no group differences. An alternative approach to BM was suggested by Albinsson *et al.* based on the expansion of the conventional technique with an additional reference block [60]. The two reference blocks originate from two consecutive frames. The evaluation of the method in *in silico*, phantom and *in vivo* data showed improved accuracy and the possibility to reduce the size of the reference blocks while maintaining the performance.

The LSME was proposed by Maurice and Bertrand [61] to describe speckle motion by following local characteristics of the speckle field. The method involves an analytical description of the decorrelation that enables the derivation of an appropriate inverse filter for speckle restoration. Assessment of tissue motion derived by this method was then used to produce elastograms of the carotid artery [62], with the additional use of von Mises coefficients to address mechanical artefacts due to different directions between tissue motion and ultrasound beam propagation. A compensative model, based on the LSME, was suggested by Mercure *et al.* to address the angle-dependence of motion estimates [63]. It was demonstrated that the model allows the estimation of scanning angle with less than 3° and 4° error, according to experiments on vessel-mimicking phantoms and in *in vivo* human carotid arteries, respectively.

Using vector velocity imaging (VVI), Svedlund and Gan [64] demonstrated that longitudinal displacements in the normal common carotid artery were significantly lower in subjects with CAD compared to healthy young adults. Svedlund and Gan also showed that carotid artery longitudinal displacements 1) were significantly lower in subjects with carotid plaque compared to age-matched controls [65], and 2) reflected cardiovascular status and predict short-term event-free survival in medium-

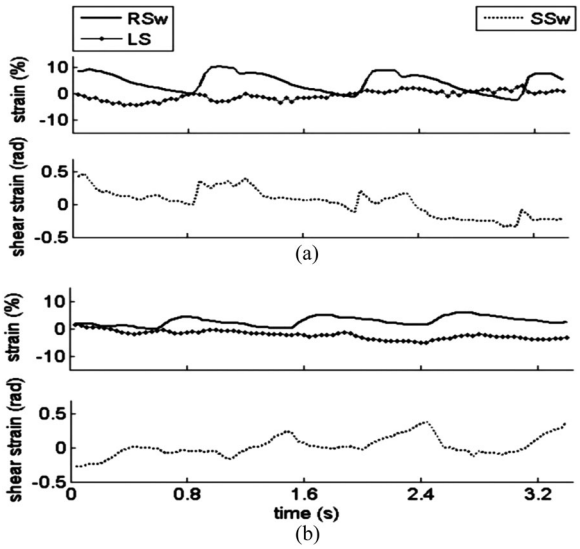

Fig. 5. Examples of strain waveforms for (a) a young and (b) an elderly normal subject. RS_W : radial strain at wall; LS: longitudinal strain; SS_W : shear strain at wall (from [67]).

to high-risk patients [66]. In [65], it was also demonstrated that, in mice, low longitudinal displacements were associated with greater intima-media thickness, greater plaque burden, and higher cholesterol levels.

In addition to BM, differential methods have also been applied to investigate motion in the carotid artery. Golemati *et al.* compared the performances of BM- and OF-based methods, in terms of *in silico* data, and suggested OF using weighted least squares as the optimal method [67]. Fig. 5 shows examples of derived strains using this method in a young and an elderly subject. Mokhtari-Dizajl *et al.* [68] used OF to estimate systolic and diastolic diameters of the right common carotid artery, proximal to plaque, from sequences of B-mode and color Doppler ultrasound images. They subsequently calculated standard arterial stiffness indices, which were found to be significantly different in subjects with severe, i.e., greater than 40%, stenosis compared to subjects with mild or no stenosis. OF was also used to produce elastograms, from B-mode, rather than from the usual RF, images of the carotid artery [69].

Recently, a noninvasive vascular elastography approach was used to quantify the strain behavior of near and far walls in longitudinal images of normal ($N = 30$) and atherosclerotic, i.e., with greater than 50% stenosis, ($N = 21$) internal carotid arteries [70]. The mean systolic, diastolic, and cumulated axial strains could distinguish the two groups after normalization by the pressure gradient between acquired images, implying that these measures may help to diagnose vulnerable plaques. Furthermore, a phase-based method was used to estimate longitudinal arterial motion *in vivo* [71] and in phantoms [72] using transverse oscillations.

E. Other Peripheral Arteries (Brachial, Femoral, Popliteal)

The motion of the brachial and popliteal arteries was estimated in a small group of subjects using BM [6]. A bidirectional

pattern of longitudinal motion and SS between intima-media and adventitia was observed, similar to those in the carotid artery and the aorta.

V. Discussion and Future Perspectives

In this paper, motion estimation methods were reviewed, which have been applied to ultrasound images of cardiovascular tissue, including the myocardium and central and peripheral arteries. Speckle tracking and modeling, and registration are the dominant methods used to calculate tissue displacements from sequences of images. Kinematic and mechanical indices are extracted from these displacements, which can provide valuable functional information about the cardiovascular system in normal and diseased conditions. An important application of motion-based strain indices involves the estimation of elastograms of the cardiovascular tissue.

The studies reviewed in this paper have shown the great potential of motion analysis in describing various aspects of the complex mechanical phenomena taking place within the cardiovascular tissue, including localized properties, along small segments of the myocardial and arterial walls, which include, among others, longitudinal-transverse anisotropy. The reported methods allow the extraction of a number of motion-derived indices for *in vivo* quantification of tissue mechanical properties, and may be valuable in disease prognosis, diagnosis, and monitoring. Such indices are important for describing properties of tissue at different times of its natural history, and, thus, for describing its vulnerability, i.e., its proneness to cause fatal events, such as heart attacks and strokes. Motion-derived indices provide functional, rather than mere anatomical information, which is more sensitive to early wall changes due to the presence of ageing or disease, which is crucial for early diagnosis. They can be used to identify novel noninvasive markers of cardiovascular risk, which will improve risk stratification and allow a more personalized disease management toward increased patient safety. Furthermore, because these indices are derived from ultrasound imaging, which is a low cost modality, they ensure not only a valid but also a cost-efficient diagnostic procedure.

Both B-mode and RF images have been used to estimate motion of heart (e.g., [27] and [33], respectively) and vessels (e.g., [7] and [37], respectively). Compared to RF images, which are only available in research-oriented devices, B-mode images are clinically (commercially) available, favoring the application of the reported methods in clinical settings. Taking advantage of the lower spatial resolution of B-mode images, a combined scheme has been suggested, in which coarse displacement estimates were obtained from B-mode images, and were subsequently used to guide the high-resolution estimates from RF data [73]. The relative performance of these two types of images in terms of estimating tissue properties has been investigated in a few studies. Ma and Varghese reported reduced variability in myocardial strain estimation when RF signals were used instead of B-mode ones [74]. On the other hand, it was recently shown that local arterial stiffness can be measured with standard B-mode scanners as reliably as with RF data [75].

Given that the full potential of the motion analysis methodologies and derived indices remains to be proven, the obvious future perspective is their application in large clinical trials. Another important future step is the combination of motion-derived indices, with 1) other motion-derived ones, 2) other ultrasound-image-based indices, including, for example, IMT and texture indices, and 3) disease biomarkers, such as biochemical indices. Such combinations will allow a more integrated and in-depth approach to arterial biomechanics.

In conclusion, ultrasound-image-based motion analysis of cardiovascular tissues has shown promise in characterizing regional mechanical properties. Its full potential in predicting, diagnosing, and monitoring disease remains to be demonstrated in large clinical trials, allowing its association with other biomarkers, toward an integrated personalized approach for CVD management.

References

[1] D. Mozaffarian *et al.*, "American heart association statistics committee and stroke subcommittee heart disease and stroke statistics—2015 update: A report from the American heart association," *Circulation*, vol. 131, no. 4, pp. e29–e322, Jan. 2015.
[2] K. S. Nikita, "Atherosclerosis: The evolving role of vascular image analysis," *Comput. Med. Imag. Graph.*, vol. 37, no. 1, pp. 1–3, Jan. 2013.
[3] A. Adji, M. F. O'Rourke, and M. Namasivayam, "Arterial stiffness, its assessment, prognostic value, and implications for treatment," *Amer. J. Hypertens.*, vol. 24, no. 1, pp. 5–17, Jan. 2011.
[4] Y. C. Fung, *Biomechanics—Mechanical Properties of Living Tissues*, 2nd ed. New York, NY, USA: Springer-Verlag, 1993.
[5] W. W. Nichols and M. F. O'Rourke, *McDonald's Blood Flow in Arteries*. London, U.K.: Arnold, 1998.
[6] M. Cinthio, Å. R. Ahlgren, J. Bergkvist, T. Jansson, H. W. Persson, and K. Lindström, "Longitudinal movements and resulting shear strain of the arterial wall," *Amer. J. Physiol. Heart Circ. Physiol.*, vol. 291, no. 1, pp. H394–H402, Jul. 2006.
[7] A. Gastounioti, S. Golemati, J. S. Stoitsis, and K. S. Nikita, "Adaptive block matching methods for carotid artery wall motion estimation from B-mode ultrasound: In silico evaluation & in vivo application," *Phys. Med. Biol.*, vol. 58, no. 24, pp. 8647–8661, Dec. 2013.
[8] S. E. Greenwald, "Ageing of the conduit arteries," *J. Pathol.*, vol. 211, no. 2, pp. 157–172, Jan. 2007.
[9] P. N. T. Wells and M. Halliwell, "Speckle in ultrasonic imaging," *Ultrasonics*, vol. 19, pp. 225–229, 1981.
[10] J. A. Hossack, "Influence of elevational motion on the degradation of 2D image frame matching," *IEEE Ultrason. Symp.*, Oct. 2000, vol. 2, pp. 1713–1716.
[11] J. Ophir, E. I. Céspedes, H. Ponnekanti, Y. Yazdi, and X. Li, "Elastography: A quantitative method for imaging the elasticity in biological tissues," *Ultrason. Imag.*, vol. 13, no. 2, pp. 111–134, Apr. 1991.
[12] E. Sanidas and G. Dangas, "Evolution of intravascular assessment of coronary," *Clin. Invest.*, vol. 43, no. 9, pp. 996–1008, Sep. 2013.
[13] Y. F. Cheung, "The role of 3D wall motion tracking in heart failure," *Nature Rev. Cardiol.*, vol. 9, no. 11, pp. 644–657, Nov. 2012.
[14] B. H. Bijnens, M. Cikes, C. Butakoff, M. Sitges, and F. Crispi, "Myocardial motion and deformation: What does it tell us and how does it relate to function?" *Fetal Diagn. Ther.*, vol. 32, nos. 1/2, pp. 5–16, 2012.
[15] E. Messas, J. L. Guerrero, M. D. Handschumacher, C.-M. Chow, S. Sullivan, E. Schwammenthal, and R. A. Levine, "Paradoxic decrease in ischemic mitral regurgitation with papillary muscle dysfunction. Insights from three-dimensional and contrast echocardiography with strain rate measurement," *Circulation*, vol. 104, no. 16, pp. 1952–1957, Oct. 2001.
[16] J. U. Voigt, B. Exner, K. Schmiedehausen, C. Huchzermeyer, U. Reulbach, U. Nixdorff, G. Platsch, T. Kuwert, W. G. Daniel, and F. A. Flachskampf, "Strain-rate imaging during dobutamine stress echocardiography provides objective evidence of inducible ischemia," *Circulation*, vol. 107, no. 16, pp. 2120–2126, Apr. 2003.
[17] T. Asanuma and S. Nakatani, "Myocardial ischaemia and post-systolic shortening," *Heart*, vol. 101, no. 7, pp. 509–516, Apr. 2015.

[18] M. S. Suffoletto, K. Dohi, M. Cannesson, S. Saba, and J. Gorcsan, "Novel speckle-tracking radial strain from routine black-and-white echocardiographic images to quantify dyssynchrony and predict response to cardiac resynchronization therapy," *Circulation*, vol. 113, no. 7, pp. 960–968, Feb. 2006.

[19] M. Dandel, H. Lehmkuhl, C. Knosalla, N. Suramelashvili, and R. Hetzer, "Strain and strain rate imaging by echocardiography—Basic concepts and clinical applicability," *Curr. Cardiol. Rev.*, vol. 5, no. 2, pp. 133–148, May 2009.

[20] A. Saltijeral *et al.*, "Early myocardial deformation changes associated to isolated obesity: A study based on 3D-wall motion tracking analysis," *Obesity*, vol. 19, no. 11, pp. 2268–2273, Jun. 2011.

[21] S. Cimino *et al.*, "Global and regional longitudinal strain assessed by two-dimensional speckle tracking echocardiography identifies early myocardial dysfunction and transmural extent of myocardial scar in patients with acute ST elevation myocardial infarction and relatively preserved LV function," *Eur. Heart J., Cardiovasc. Imag.*, vol. 14, pp. 805–811, 2013.

[22] N. Duchateau *et al.*, "Myocardial motion and deformation patterns in an experimental swine model of acute LBBB/CRT and chronic infarct," *Int. J. Cardiovasc. Imag.*, vol. 30, no. 5, pp. 875–887, Jun. 2014.

[23] L. Gong *et al.*, "Assessment of myocardial viability in patients with acute myocardial infarction by two-dimensional speckle tracking echocardiography combined with low-dose dobutamine stress echocardiography," *Int. J. Cardiovasc. Imag.*, vol. 29, no. 5, pp. 1017–1028, Jan. 2013.

[24] M. Alessandrini, A. Basarab, H. Liebgott, and O. Bernard, "Myocardial motion estimation from medical images using the monogenic signal," *IEEE Trans. Image Process.*, vol. 22, no. 3, pp. 1084–1095, Mar. 2013.

[25] A. H. Curiale, G. Vegas-Sánchez-Ferrero, J. G. Bosch, and S. Aja-Fernández, "A maximum likelihood approach to diffeomorphic speckle tracking for 3D strain estimation in echocardiography," *Med. Image Anal.*, vol. 24, no. 1, pp. 90–105, May 2015.

[26] N. Duchateau *et al.*, "A spatiotemporal statistical atlas of motion for the quantification of abnormal myocardial tissue velocities," *Med. Image Anal.*, vol. 15, no. 3, pp. 316–328, Jun. 2011.

[27] B. Heyde *et al.*, "Elastic image registration versus speckle tracking for 2-D myocardial motion estimation: A direct comparison in vivo," *IEEE Trans. Med. Imag.*, vol. 32, no. 2, pp. 449–459, Feb. 2013.

[28] S. Langeland *et al.*, "Experimental assessment of a new research tool for the estimation of two-dimensional myocardial strain," *Ultrasound Med. Biol.*, vol. 32, no. 10, pp. 1509–1513, Oct. 2006.

[29] M. De Craene *et al.*, "Temporal diffeomorphic free-form deformation: Application to motion and strain estimation from 3-D echocardiography," *Med. Image Anal.*, vol. 16, no. 2, pp. 427–450, Feb. 2012.

[30] Y. Zhang, Y. Gao, J. Jiao, X. Li, S. Li, and J. Yang, "Robust boundary detection and tracking of left ventricles on ultrasound images using active shape model and ant colony optimization," *Biomed. Mater. Eng.*, vol. 24, no. 6, pp. 2893–2899, 2014.

[31] J.G. Bosch, S.C. Mitchell, B.P. Lelieveldt, F. Nijland, O. Kamp, M. Sonka, and J. H. Reiber, "Automatic segmentation of echocardiographic sequences by active appearance motion models," *IEEE Trans. Med. Imag.*, vol. 21, no. 11, pp. 1374–1383, Nov. 2002.

[32] J.G. Bosch, F. Nijland, S. C. Mitchell, B. P. Lelieveldt, O. Kamp, J. H. Reiber, and M. Sonka, "Computer-aided diagnosis via model-based shape analysis: Automated classification of wall motion abnormalities in echocardiograms," *Acad. Radiol.*, vol. 12, no. 3, pp. 358–367, Mar. 2005.

[33] W.-N. Lee and E. E. Konofagou, "Angle-independent and multi-dimensional myocardial elastography—From theory to clinical validation," *Ultrasonics*, vol. 48, nos. 6/7, pp. 563–567, Nov. 2008.

[34] W.-N. Lee, J. Provost, K. Fujikura, J. Wang, and E. E. Konofagou, "In vivo study of myocardial elastography under graded ischemia conditions," *Phys. Med. Biol.*, vol. 56, no. 4, pp. 1155–1172, Feb. 2011.

[35] S. J. Okrasinski, B. Ramachandran, and E. E. Konofagou, "Assessment of myocardial elastography performance in phantoms under combined physiologic motion configurations with preliminary in vivo feasibility," *Phys. Med. Biol.*, vol. 57, no. 17, pp. 5633–5650, Sep. 2012.

[36] J. Luo and E. E. Konofagou, "A fast normalized cross-correlation calculation method for motion estimation," *IEEE Trans. Ultrason., Ferroelectr., Freq. Control*, vol. 57, no. 6, pp. 1347–1357, Jun. 2010.

[37] J. Luo and E. E. Konofagou, "Imaging of wall motion coupled with blood flow velocity in the heart and vessels in vivo: A feasibility study," *Ultrasound Med. Biol.*, vol. 37, no. 6, pp. 980–995, Jun. 2011.

[38] A. Danpinid, J. Luo, J. Vappou, P. Terdtoon, and E. E. Konofagou, "*In vivo* characterization of the aortic stress-strain relationship," *Ultrasonics*, vol. 50, no. 7, pp. 654–665, Jun. 2010.

[39] T. Khamdaeng, J. Luo, J. Vappou, P. Terdtoon, and E. E. Konofagou, "Arterial stiffness identification of the human carotid artery using the stress-strain relationship in vivo," *Ultrasonics*, vol. 52, no. 3, pp. 402–411, Mar. 2012.

[40] C. L. de Korte, G. Pasterkamp, A. F. W. van der Steen, H. A. Woutman, and N. Bom, "Characterization of plaque components with intravascular ultrasound elastography in human femoral and coronary arteries in vivo," *Circulation*, vol. 102, no. 6, pp. 617–623, Aug. 2000.

[41] J. A. Schaar *et al.* "Characterizing vulnerable plaque features with intravascular elastography," *Circulation*, vol. 108, no. 21, pp. 2636–2641, Nov. 2003.

[42] R. L. Maurice, J. Ohayon, G. Finet, and G. Cloutier, "Adapting the Lagrangian speckle model estimator for endovascular elastography: Theory and validation with simulated radio-frequency data," *J. Acoust. Soc. Amer.*, vol. 116, no. 2, pp. 1276–1286, Aug. 2004.

[43] R. L. Maurice, J. Fromageau, E. Brusseau, G. Finet, G. Rioufol, and G. Cloutier, "On the potential of the Lagrangian estimator for endovascular ultrasound elastography: In vivo human coronary artery study," *Ultrasound Med. Biol.*, vol. 33, no. 8, pp. 1199–1205, Aug. 2007.

[44] S. Le Floc'h *et al.*, "A four-criterion selection procedure for atherosclerotic plaque elasticity reconstruction based on in vivo coronary intravascular ultrasound radial strain sequences," *Ultrasound Med. Biol.*, vol. 38, no. 12, pp. 2084–2097, Dec. 2012.

[45] Y. Liang, H. Zhu, and M. H. Friedman, "Estimation of the transverse strain tensor in the arterial wall using IVUS image registration," *Ultrasound Med. Biol.*, vol. 34, no. 11, pp. 1832–1845, Nov. 2008.

[46] Y. Liang, H. Zhu, T. Gehrig, and M. H. Friedman, "Measurement of the transverse strain tensor in the coronary arterial wall from clinical intravascular ultrasound images," *J. Biomech.*, vol. 41, no. 14, pp. 2906–2911, Oct. 2008.

[47] Y. Liang, H. Zhu, and M. H. Friedman, "The correspondence between coronary arterial wall strain and histology in a porcine model of atherosclerosis," *Phys. Med. Biol.*, vol. 54, no. 18, pp. 5625–5641, Sep. 2009.

[48] Y. Liang, H. Zhu, T. Gehrig, and M. H. Friedman, "Measurement of the 3D arterial wall strain tensor using intravascular B-mode ultrasound images: A feasibility study," *Phys. Med. Biol.*, vol. 55, no. 21, pp. 6377–6394, Nov. 2010.

[49] S. Golemati, A. Sassano, M. J. Lever, A. A.Bharath, S. Dhanjil, and A. N. Nicolaides, "Motion analysis of carotid atherosclerotic plaque from B-mode ultrasound," *Ultrasound Med. Biol.*, vol. 29, no. 3, pp. 387–399, Mar. 2003.

[50] M. Cinthio, Å. R. Ahlgren, J. T. Jansson, A. Eriksson, H. W. Persson, and K. Lindström, "Evaluation of an ultrasonic echo-tracking method for measurements of arterial wall movements in two dimensions," *IEEE Trans. Ultrason., Ferroelectr., Freq. Contr.*, vol. 52, no. 8, pp. 1300–1311, Aug. 2005.

[51] M. Cinthio and Å. R. Ahlgren, "Intra-observer variability of longitudinal displacement intramural shear strain measurements of the arterial wall using ultrasound noninvasively in vivo," *Ultrasound Med. Biol.*, vol. 36, no. 5, pp. 697–704, May 2010.

[52] G. Zahnd *et al.*, "Measurement of two-dimensional movement parameters of the carotid artery wall for early detection of arteriosclerosis: A preliminary clinical study," *Ultrasound Med. Biol.*, vol. 37, no. 9, pp. 1421–1429, Sep. 2011.

[53] G. Zahnd *et al.*, "Longitudinal displacement of the carotid wall and cardiovascular risk factors: Associations with aging, adiposity, blood pressure and periodontal disease independent of cross-sectional distensibility and intima-media thickness," *Ultrasound Med. Biol.*, vol. 38, no. 10, pp. 1705–1715, Oct. 2012.

[54] E. Soleimani, M. Mokhtari-Dizaji, and H. Saberi, "A novel non-invasive ultrasonic method to assess total axial stress of the common carotid artery wall in healthy and atherosclerotic men," *J. Biomech.*, vol. 48, no. 10, pp. 1860–1867, Jul. 2015.

[55] A. Gastounioti, S. Golemati, J. Stoitsis, and K. S. Nikita, "Comparison of Kalman-filter-based approaches for block matching in arterial wall motion analysis from B-mode ultrasound," *Meas. Sci. Technol.*, vol. 22, no. 11, Oct. 2011.

[56] Α. Gastounioti, S. Makrodimitris, S. Golemati, N. P. E. Kadoglou, C. D. Liapis, and K. S. Nikita, "A novel computerized tool to stratify risk in carotid atherosclerosis using kinematic features of the arterial wall," *IEEE J. Biomed. Health Informat.*, vol. 19, no. 3, pp. 1137–1145, May 2015.

[57] G. Zahnd, M. Orkisz, A. Sérusclat, P. Moulin, and D. Vray, "Evaluation of a Kalman-based block matching method to assess the bi-dimensional motion of the carotid artery wall in B-mode ultrasound sequences," *Med. Image Anal.*, vol. 17, no. 5, pp. 573–585, Jul. 2013.

[58] G. Zahnd, S. Balocco, A. Sérusclat, P. Moulin, M. Orkisz, and D. Vray, "Progressive attenuation of the longitudinal kinetics in the common carotid artery: Preliminary in vivo assessment," *Ultrasound Med. Biol.*, vol. 41, no. 1, pp. 339–345, Jan. 2015.

[59] J. Tat, J. S. Au, P. J. Keir, and M. J. MacDonald, "Reduced common carotid artery longitudinal wall motion and intramural shear strain in individuals with elevated cardiovascular disease risk using speckle tracking," *Clin. Physiol. Funct. Imag.*, Jul. 2015, doi: 10.1111/cpf.12270.

[60] J. Albinsson, S. Brorsson, Å. R. Ahlgren, and M. Cinthio, "Improved tracking performance of Langrangian block-matching methodologies using block expansion in the time domain: In silico, phantom and in vivo evaluations," *Ultrasound Med. Biol.*, vol. 40, no. 10, pp. 2508–2520, Oct. 2014.

[61] R. L. Maurice and M. Bertrand, "Langrangian speckle model and tissue-motion estimation-theory," *IEEE Trans. Med. Imag.*, vol. 18, no. 7, pp. 593–603, Jul. 1999.

[62] R. L. Maurice, J. Ohayon, Y. Frétigny, M. Bertrand, G. Soulez, and G. Cloutier, "Noninvasive vascular elastography: Theoretical framework," *IEEE Trans. Med. Imag.*, vol. 23, no. 2, pp. 164–180, Feb. 2004.

[63] E. Mercure, J. F. Deprez, J. Fromageau, O. Basset, G. Soulez, G. Cloutier, and R. L. Maurice, "A compensative model for the angle-dependence of motion estimates in noninvasive vascular elastography," *Med. Phys.*, vol. 38, no. 2, pp. 727–735, Feb. 2011.

[64] S. Svedlund and L. M. Gan, "Longitudinal wall motion of the common carotid artery can be assessed by velocity vector imaging," *Clin. Physiol. Funct. Imag.*, vol. 31, pp. 332–338, 2011.

[65] S. Svedlund and L. M. Gan, "Longitudinal common carotid artery wall motion is associated with plaque burden in man and mouse," *Atherosclerosis*, vol. 217, no. 1, pp. 120–124, Jul. 2011.

[66] S. Svedlund, C. Eklund, P. Robertsson, M. Lomsky, and L. M. Gan, "Carotid artery longitudinal displacement predicts 1-year cardiovascular outcome in patients with suspected coronary artery disease," *Arteriosclerosis Thrombosis Vasc. Biol.*, vol. 31, no. 7, pp. 1668–1674, Jul. 2011.

[67] S. Golemati, J. S. Stoitsis, A. Gastounioti, A. C. Dimopoulos, V. Koropouli, and K. S. Nikita, "Comparison of block matching and differential methods for motion analysis of the carotid artery wall from ultrasound images," *IEEE Trans. Inf. Technol. Biomed.*, vol. 16, no. 5, pp. 852–858, Sep. 2012.

[68] M. Mokhtari-Dizajl, M. Montazeri, and H. Saberi, "Differentiation of mild and severe stenosis with motion estimation in ultrasound images," *Ultrasound Med. Biol.*, vol. 32, no. 10, pp. 1493–1498, Oct. 2006.

[69] T. Zakaria, Z. Qin, and R. L. Maurice, "Optical-flow-based B-mode elastography: Application in the hypertensive rat carotid," *IEEE Trans. Med. Imag.*, vol. 29, no. 2, pp. 570–578, Feb. 2010.

[70] E. Mercure, F. Destrempes, M. H. Roy Cardinal, J. Porée, G. Soulez, J. Ohayon, and G. Cloutier, "A local angle compensation method based on kinematics constraints for non-invasive vascular axial strain computations on human carotid arteries," *Comput. Med. Imag. Graph.*, vol. 38, no. 2, pp. 123–136, Mar. 2014.

[71] G. Zahnd, S. Salles, H. Liebgott, D. Vray, A. Sérusclat, and P. Moulin, "Real-time ultrasound-tagging to track the 2D motion of the common carotid artery in vivo," *Med. Phys.*, vol. 42, no. 2, pp. 820–830, Feb. 2015.

[72] S. Salles, A. J. Chee, D. Garcia, A. C. Yu, D. Vray, and H. Liebgott, "2-D arterial wall motion imaging using ultrafast ultrasound and transverse oscillations," *IEEE Trans. Ultrason., Ferroelectr., Freq. Control*, vol. 62, no. 6, pp. 1047–1058, Jun. 2015.

[73] H. Shi and T. Varghese, "Two-dimensional multi-level strain estimation for discontinuous tissue," *Phys. Med. Biol.*, vol. 52, no. 2, pp. 389–401, Jan. 2007.

[74] C. Ma and T. Varghese, "Comparison of cardiac displacement and strain imaging using ultrasound radiofrequency and envelope signals," *Ultrasonics*, vol. 53, no. 3, pp. 782–792, Mar. 2013.

[75] J. Steinbuch, A. P. Hoeks, E. Hermeling, M. T. Truijman, F. H. Schreuder, and W. H. Mess, "Standard B-mode ultrasound measures local carotid artery characteristics as reliably as radiofrequency phase tracking in symptomatic carotid artery patients," *Ultrasound Med. Biol.*, vol. 42, no. 2, pp. 586–595, Feb. 2016.

[76] EngrApps.com. (2016, Feb. 4). Arterial stresses. [Online]. Available: http://engrapps.com/mechanical-systems-and-materials/mechanical-components/pressure-vessels/burst-collapse-analysis.php

Authors' photographs and biographies not available at the time of publication.